Journal of Physics: Conference Series

High Pressure optical nanothermometer based on Er^{3+} photoluminescence

High Pressure optical nanothermometer based on Er^{3+} photoluminescence

V Gutiérrez-Cano[1*], R Valiente[2], J A González[1] and F Rodríguez[1*]

[1]Malta Consolider Team, DCITIMAC, Facultad de Ciencias, University of Cantabria, Av. de los Castros s/n, Santander 39005, Spain
[2] Applied Physics Department – Nanomedicine Group, University of Cantabria-IDIVAL, 39005, Santander, Spain

rodriguf@unican.es

Abstract. The optical properties of a sparsely investigated material, $LaGdO_3$ doped with Er^{3+}, are explored regarding its suitability as nanothermometer. Besides its excellent capabilities for dielectric applications, when doping with Er^{3+}, this material provides a highly efficient up-conversion photoluminescence (PL) for high temperature thermometry at high pressure due to its structural stability. $LaGdO_3$ belongs to the perovskite-type ABO_3 compounds with a B-type monoclinic $C2/m$ space group (a = 14.43 Å; b = 3.69 Å; c = 9.00 Å; and β = 100.70º) at ambient conditions. It undergoes a structural phase transition to a hexagonal $P\bar{3}m1$ phase at 3 GPa yielding a notable PL enhancement, thus enabling it as a potential high-pressure high-temperature nanothermometer.

1. Introduction

Spectroscopic thermometry based on narrow photoluminescence (PL) lines is a rapidly developing field worthy for applications in systems under special environmental conditions of pressure and temperature [1]. Ruby is an archetype of such optical probes. However, its use is limited to the low temperature range (< 150 K), which is mainly determined by the thermal coupling of the two R-lines (ΔE = 29 cm^{-1}), material stability and PL efficiency [2]. In this work we present an oxide material, $LaGdO_3$ that, besides its excellent capabilities for dielectric applications [3], when doping with Er^{3+}, has the potential of a highly efficient up-conversion PL for high temperature thermometry at high pressure [4]. $LaGdO_3$ belongs to the perovskite-type ABO_3 compounds with a B-type monoclinic $C2/m$ space group (a = 14.43 Å; b = 3.69 Å; c = 9.00 Å; and β = 100.70º) at ambient conditions [5]. It undergoes a structural phase transition to a hexagonal phase at 4 GPa yielding PL enhancement. Since the energy gap of the thermalized $^2H_{11/2}$ and $^4S_{3/2}$ Er^{3+} levels (ΔE = 732 cm^{-1}) is nearly constant with pressure, the intensity ratio between the emission from both states to the $^4I_{15/2}$ ground state makes it suitable for high-temperature high-pressure applications (T > 1100 K). Here, we present a thoroughly study of its structure, vibrational and electronic properties that will be compared with the isostructural compound $SmGdO_3$, showing a structural phase transition around 3 GPa [6].

2. Experimental methods

2.1. Synthesis

$LaGdO_3$ powders were synthesized via sol-gel Pechini method using $La(NO_3)_3{\cdot}6H_2O$ (99.9%), $Gd(NO_3)_3{\cdot}6H_2O$(99.9%), $Er(NO_3)_3{\cdot}6H_2O$ (99.9%), citric acid (99%) -from Alfa Aesar- and polyethylene glycol 10000 -from Merck- as starting materials. The obtained sol was heated at 90 °C for 24 h to form the gel, and then calcined at 1200 °C for 8h. This synthesis conditions yielded nanocrystal sizes in the 45– 70 nm range. For pressure experiments, we used $LaGdO_3$ nanocrystals with Er^{3+} concentration of 1 mol%. Its B-type monoclinic *C2/m* structure was checked by x-ray diffraction with lattice parameters: a = 14.459(2) Å; b = 3.699(1) Å; c = 9.021(1) Å; and β = 100.7(1)º (V = 474.0(4) Å^3), at ambient conditions.

2.2. Spectroscopic measurements

Luminescence spectra were acquired in a Horiba-Jobin-Yvon T64000 Raman spectrometer equipped with a nitrogen-cooled CCD and a confocal microscope for detection. The 488 nm line of a coherent Innova Spectrum 70C Ar^+-Kr^+ laser was used as excitation source. Temperature dependent measurements in the 298-873 K range were performed with a heating stage Linkam TS1000 coupled to the T64000 spectrometer, using a 20× objective and a laser power output of 1 mW on sample. The intensity-to-temperature calibration procedure was performed by placing the nanocrystals in thermal contact with the temperature controller during 5 min for each temperature step before collecting the emission spectrum.

2.3. High pressure

High-pressure experiments were carried out in a membrane diamond anvil cell (DACs). The 200 μm thickness Inconel gaskets were preindented to 40-70 μm. The hydrostatic chamber consists of a 150 μm diameter hole perforated in the gasket with a BETSA motorized electrical discharge machine. The DAC was loaded with suitable Er^{3+}-doped $LaGdO_3$ nanocrystals and ruby microspheres (10-20 μm diameter) as pressure probes. Paraffin oil was used as pressure transmitting medium and protect sample from moisture. In all experiments, the hydrostaticity of pressure-transmitting media was checked through the broadening of the ruby R-lines.

3. Results and discussion

Figure 1 shows the PL spectra of 1 mol% Er^{3+}-doped $LaGdO_3$ nanocrystals in the green spectral region as a function of temperature (298-873 K) under 488 nm laser excitation. The green emission consists of several bands between 515 and 570 nm corresponding to transitions from $^2H_{11/2}$ and $^4S_{3/2}$ excited states to the $^4I_{15/2}$ ground state of Er^{3+}, respectively. As these two excited states are thermally coupled, their emission intensity ratio, *FIR*, depends on the respective excited-state equilibrium populations, which are governed by the Boltzmann distribution:

$$FIR = \frac{I_{525}}{I_{549}} = C\, e^{-\Delta E/kT} \qquad (1)$$

where I_{525} and I_{549} are the integrated intensities of the two thermally-coupled multiplets, C is a constant that depends on the state degeneracy, spontaneous emission rates, branching ratio, and photon energies of the emitting states in the host material, ΔE is the energy gap between the $^2H_{11/2}$ and $^4S_{3/2}$ multiplets, –both C and ΔE are characteristic of each material host–, k is the Boltzmann constant, and T is the absolute temperature.

The temperature dependence of the luminescence can be easily obtained by least-square fitting of the experimental ln(*FIR*) *vs*. 1/*T* data to a linear equation, the slope of which gives $\Delta E/k$ and the ln(*FIR*) intercept, ln(*C*) (Eq. 1). These two parameters provide the thermometric scale (Fig. 1c) with values of ΔE = 732 ± 5 cm^{-1} (90.7 ± 0.9 meV) and C = 8.25 ± 0.12 [7]. The so-obtained energy gap coincides with that measured spectroscopically from the $^2H_{11/2}$ and $^4S_{3/2}$ centroid positions. Due to the weak crystal-field dependence of these transitions, the obtained gap in $LaGdO_3$: Er^{3+} is also comparable to that obtained in other reported compounds like fluorotellurite glass doped with Er^{3+} (810 cm^{-1}) [8],

$LiNbO_3$: Er^{3+}/Yb^{3+} (869 cm^{-1}) [9] and $NaY(MoO_4)_2$: Er^{3+}/Yb^{3+}(736 cm^{-1}) [10], and $NaYF_4$: Er^{3+}/Yb^{3+}(714 cm^{-1}) [11]. To better illustrate the suitability of 1 mol% Er^{3+}-doped $LaGdO_3$ nanocrystals as a sensor for optical thermometry, its performance and temperature range of operation with different Er^{3+}-based host materials is evaluated through their absolute (S) and relative (S_R) sensitivities. These parameters can be deduced from eq. (1) as:

$$S = \left|\frac{\partial FIR}{\partial T}\right| = FIR\ \frac{\Delta E}{kT^2} \quad (2)$$

$$S_R = \left|\frac{1}{FIR}\frac{\partial FIR}{\partial T}\right| = \frac{\Delta E}{kT^2} \quad (3)$$

The obtained values for 1 mol% Er^{3+}-doped $LaGdO_3$ are shown in Fig. 1d as a function of temperature. The highest sensitivity is found at T= 554 K with S= 4.3×10^{-3} K^{-1}, while the highest relative sensitivity S_R is at 0 K and decreases with temperature reaching a value of 1.2×10^{-2} K^{-1} at 298 K and 0.1×10^{-2} K^{-1} at 900 K. Interestingly, this host material provides one of the largest-ever temperature range of operation without any further surface modification.

These performances are very competitive when compared with other well-stablished Er^{3+}-based optical thermometers in different fluoride and oxide hosts. Table 1 compares sensitivity values measured in different crystal and glass hosts, which are known to be efficient at high temperature.

Table 1. Comparison of thermometric properties in Er^{3+}/Yb^{3+}-doped luminescent materials: energy gap between the $^2H_{11/2}$ and $^4S_{3/2}$ multiplets (ΔE), absolute sensitivity (S), in parenthesis the maximum sensitivity temperature, and temperature range of operation.

Sensing Material	ΔE ($^2H_{11/2} - {}^4S_{3/2}$) cm^{-1} (meV)	S (10^{-3} K^{-1})	Temperature range (K)	Reference
$LaGdO_3$: 1 mol% Er^{3+}	732 (90.7)	4.3 (554 K)	298-873	7
fluorotellurite glass: Er^{3+}	810 (100)	8 (541)	100-573	8
$LiNbO_3$: Er^{3+}/Yb^{3+}	869 (108)	14 (350 K)	293-450	9
$NaY(MoO_4)_2$: Er^{3+}/Yb^{3+}	736 (91.3)	15.5 (530 K)	298-700	10
$NaYF_4$: Er^{3+}/Yb^{3+}	714 (88.5)	2.4 (554 K)	300-700	11

It must be noted that the $LaGdO_3$ host matrix provides the widest temperature range of operation although its absolute sensitivity is moderate. This characteristic enables this material as a potential highly-efficient high-temperature optical thermometer, even in the nanoscale where melting temperatures are expected to be lower than in bulk.

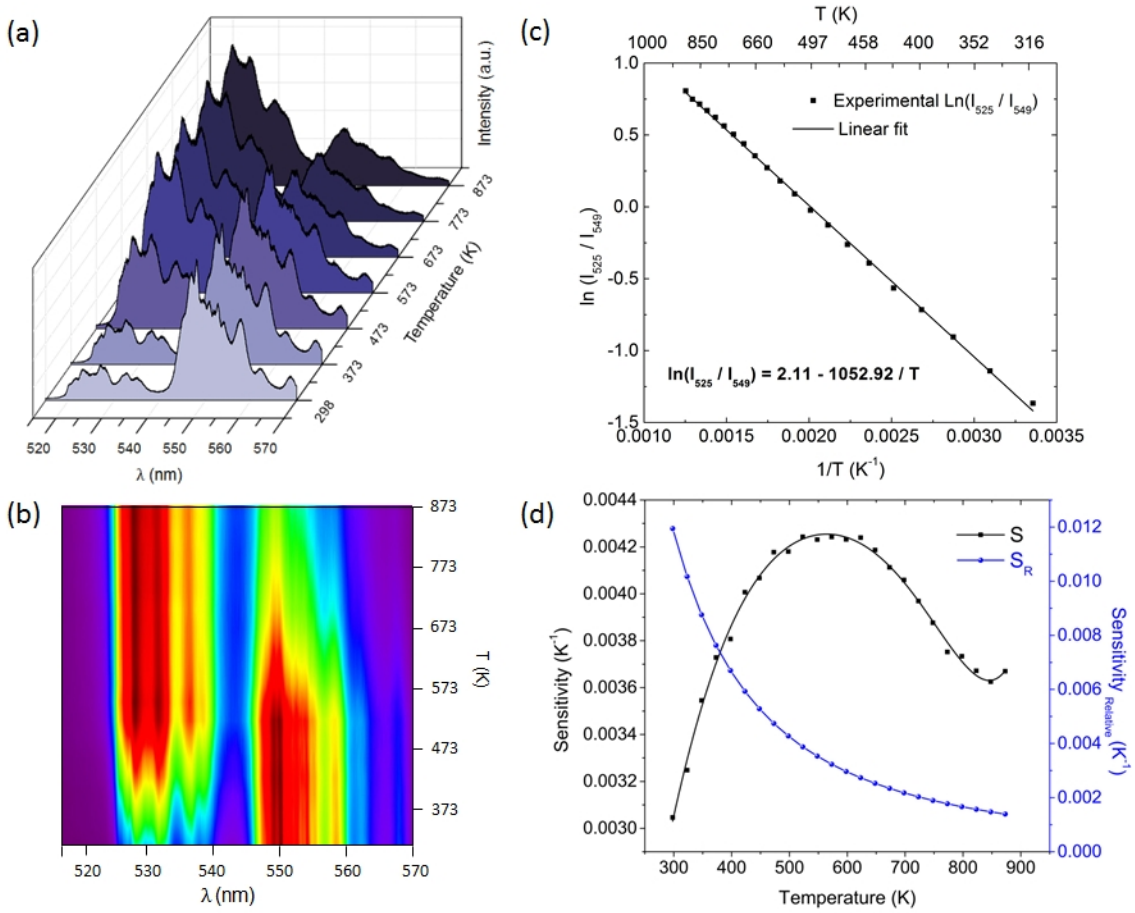

Figure 1. Temperature sensing properties of 1 mo% Er^{3+}-doped $LaGdO_3$ nanocrystals under λ = 488 nm laser excitation. (a) Emission spectra as a function of the absolute temperature; (b) intensity contour plots of the emission spectra vs. temperature; (c) semilog plot of the FIR as a function of the reciprocal absolute temperature; (d) sensor absolute (in black) and relative (in blue) sensitivities as a function of temperature. Reprinted with permission from [7]. Copyright (2019) American Chemical Society.

The pressure dependence of the PL spectrum in the red spectral region is shown in Fig. 2. The PL emission corresponds to the electric-dipole transition from the $^4F_{9/2}$ excited state to the $^4I_{15/2}$ ground state of Er^{3+}. The evolution of the spectrum foresees a pressure-induced structural phase transition at 4 GPa, as it is clearly evidenced by the splitting of the 565 nm line which comes into a single peak above this transition pressure. However, the main spectral features remain in both low-pressure and high-pressure phases, reflecting that these transitions are weakly dependent to changes of crystal field induced by structural transformations. Furthermore, the phase-transition occurrence has been also confirmed by Raman spectroscopy, thus indicating that, analogously to the isomorphous compound $SmGdO_3$ [6], $LaGdO_3$ also transforms to the hexagonal hexagonal $P\bar{3}m1$ phase at 4 GPa. Interestingly, this phase transition enhances the PL intensity by a factor 3, thus making it a more efficient material for thermometry.

Figure 3 shows the pressure dependence of the Er^{3+} PL spectrum in the green spectral region, which is important for thermometry. Any spectral variation of Er^{3+} in this range may influence parameters ΔE and C of eq.(1), hence the reading temperature. Therefore, a detailed analysis of the spectral variation is essential to define a proper thermometer under high-pressure conditions.

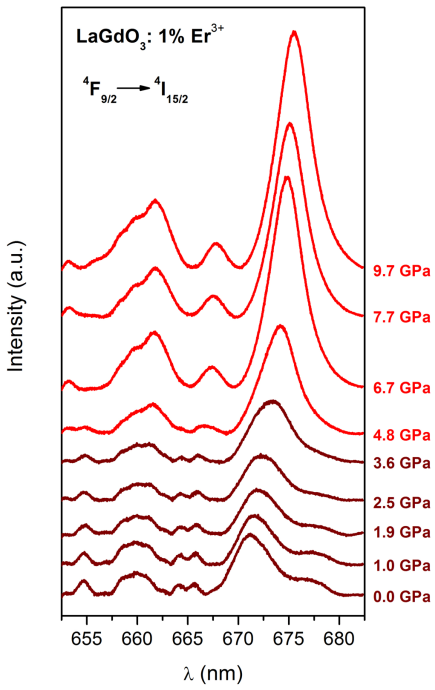

Figure 2. Red luminescence spectra of Er^{3+}-doped $LaGdO_3$ nanocrystals corresponding to the $^4F_{9/2} \rightarrow {}^4I_{15/2}$ transition at several pressures. Luminescence from the monoclinic $C2/m$ phase is shown in maroon while luminescence from hexagonal $P\bar{3}m1$ phase is shown in red.

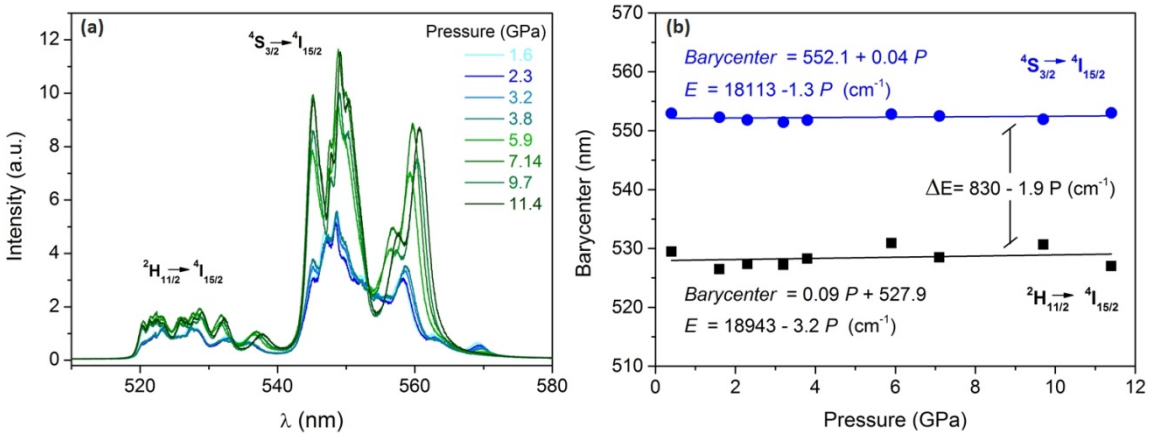

Figure 3. (a) Green luminescence spectra of Er^{3+}-doped $LaGdO_3$ nanocrystals corresponding to transitions $^2H_{11/2} \rightarrow {}^4I_{15/2}$ and $^4S_{3/2} \rightarrow {}^4I_{15/2}$ as a function of the pressure up to 11.4 GPa. The luminescence arising from the monoclinic $C2/m$ phase is shown in blue while luminescence from hexagonal $P\bar{3}m1$ phase is shown in green. (b) Variation of the barycenter of both luminescence bands as a function of pressure. Note that ΔE corresponds to the difference between barycenters, the position of which are expressed in nm (*Barycenter*) and cm^{-1} (E) in the plot.

A relevant feature related to the structural phase transition of the host matrix concerns the enhancement of Er^{3+} luminescence. The intensity of both red (Fig. 2) and green (Fig. 3) emissions, is largely enhanced in the high–pressure hexagonal $P\bar{3}m1$ phase.
Similar to $NaYF_4$, hexagonal phase is suitable for enhancing Er^{3+} luminescence with respect to the cubic phase [12]. In hexagonal $LaGdO_3$, both green and red PL intensities are almost doubled on passing from the low-pressure to the high-pressure phase. The increase in intensity, attained at the phase transition onset, actually takes place 1 GPa above the phase transition pressure determined from XRD and Raman spectroscopy [3, 13, 14]. Interestingly, the pressure-dependence of the barycenter of the green-yellow emission bands (Fig. 3.b.) is very weak, both barycenters behaving as:

$$\lambda_{^4S_{3/2}} = 552.1 + 0.040P \quad (4)$$

$$\lambda_{^2H_{11/2}} = 527.9 + 0.089P \quad (5)$$

Figure 3 shows both PL pressure dependences through which we can determine the variation of the energy gap between thermalized levels $^2H_{11/2}$ and $^4S_{3/2}$ as (in cm^{-1} and GPa units):

$$\Delta E(^2H_{\frac{11}{2}} - {}^4S_{\frac{3}{2}}) = 830 - 1.9P \quad (6)$$

It must be noted that the spectroscopic energy gap at zero pressure of ΔE = 830 cm^{-1} differs from that obtained from the ln(*FIR*) *vs*. 1/T equation fit. The distinct procedure to get ΔE yields different values since both thermalized states in Er^{3+} consist of several lines, which are all intensity averaged to obtain their barycentre. Although both energy gaps are similar, the observed difference must be ascribed to the distinct method of analysis: through spectroscopic positions (*barycenter*) and line intensities (*FIR*). Nevertheless, the pressure coefficient deduced by either method should be the same. The variation of the barycentre with pressure is small (-1.9 $cm^{-1}GPa^{-1}$) and shows a linear dependence. It means that measuring temperature by this method at high pressure implies a simple linear correction to the energy gap as $\Delta E = 720 - 1.9P$, in Eq. (1). Interestingly, the variation of the PL energy – barycentre position– for the two levels is barely affected by the structural phase transition at 4 GPa –it does not produce any detectable change in their barycentre–, and yields enhancement of the PL intensity. Thus, this material has important applications as nanothermometer under high-pressure and high-temperature conditions, since the energy gap varies little with pressure, and this variation can be easily incorporated to Eq.(1). In this way, it must be noted that the relative variation of ΔE would be less than 2% at 10 GPa, but such a variation can be easily corrected using the pressure coefficient of Eq.(6) into Eq.(1). Furthermore, the increase of PL intensity above 4 GPa improves the *FIR* sensitivity (Eq.(1)). Both features make it this material suitable for an accurate measure of the temperature at high pressure.

4. Conclusions

We have shown that Er^{3+}-doped $LaGdO_3$ nanocrystals constitute an efficient PL material for nanothermometry at high temperature (> 800 K). The PL can be excited directly with visible light or with infrared light via upconversion processes, the latter excitation being of interest in biological systems. We also showed that $LaGdO_3$ nanocrystals experience a pressure-induced monoclinic to hexagonal structural phase transition at 4 GPa yielding PL enhancement. Although this structural phase transition modifies the PL efficiency, it has a negligible effect on the energy gap governing the thermometric properties of this material. In fact, its energy gap –main spectroscopic parameter for Er^{3+}-based thermometry– depends slightly on pressure (-1.9 $cm^{-1}GPa^{-1}$), thus enabling it as a potential high-pressure high-temperature nanothermometer in the 0 – 10 GPa range.

Acknowledgements

We acknowledge financial support from MAT2015-69508-P (MINECO/FEDER), MAT2015-71070-REDC; PGC2018-101464-B-I00 (MICIN/FEDER), IDIVAL 18/28, the European

Research Council FET-OPEN NCLas H2020 Project (EU829161), and BSH Electrodomésticos España, S.A.

References

[1] Quintanilla M and Liz-Marzan L M 2018 *Nano Today* **19** 126.
[2] Datchi F, Dewaele A, Loubeyre P, Letoullec R,Le Godec Y, and B. Canny 2007 *High Pressure Research* **27(**4) 447.
[3] Pavunny S P, Pavunny S P, Thomas R, Murari N M, Schubert J, Niessen V, Luptak R, Kalkur T S, and Katiyar R S 2011 *Integr. Ferroelectr.* **125** 44.
[4] Siaï A, Haro-Gonzalez P, Naifer K H, and Férid M 2018 *Opt. Mater.* **76** 34.
[5] Pavunny S P, Kumar A, Misra P, Scott J. F, and Katiyar R S 2014 *Phys. Status Solidi (b)* **251** 131.
[6] SharmaY, Sahoo S, Mishra A K, Misra P, Pavunny S P, Dwivedi A, Sharma S M, and Katiyar R S 2015 *J. Appl. Phys.* **117** 094101.
[7] Gutierrez-Cano V, Rodriguez F, Gonzalez J A, and Valiente 2019 *J. Phys. Chem. C* **123** 29818.
[8] León-Luis S F, Rodríguez-Mendoza U R, Martín I R, Lalla E, Lavín V 2013 *Sens. Actuators B* **176**, 1167.
[9] Quintanilla M, Cantelar E, Cusso F, Villegas M, Caballero A C 2011 *Appl. Phys. Express* **4** 022601.
[10] Yang X, Fu Z, Yang Y, Zhang C, Wu Z, and Sheng T 2015 *J. Am. Ceram. Soc.* **98** 2595.
[11] Jiang S, Zeng P, Liao L, Tian S, Guo H, Chen Y, Duan C, and Yin M 2014 *J. Alloys Compd.* **617** 538.
[12] Renero-Lecuna C, Martín-Rodríguez R, Valiente R, González J, Rodríguez F, Kramer K W, Güdel H U 2011 *Chem. Mater.* **23** 3442.
[13] Wenhui S, Daiming W U, Xiaoyuan L I, Xianfeng M A, Jianshi Z, Zhengnan Q, Yifeng W, Weina L, Zhongjiu G E 1986 *Phys. B + C* **139–140** 658.
[14] Gutierrez-Cano V 2019 *PhD Thesis* University of Cantabria.